Nano Energy (2015) 16, 357–366

Available online at www.sciencedirect.com

ScienceDirect

journal homepage: www.elsevier.com/locate/nanoenergy

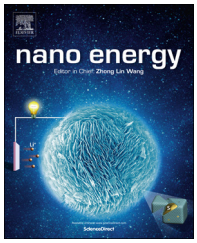

RAPID COMMUNICATION

Sulfur and nitrogen self-doped carbon nanosheets derived from peanut root nodules as high-efficiency non-metal electrocatalyst for hydrogen evolution reaction

Yucheng Zhou[a,1], Yanhua Leng[b,c,1], Weijia Zhou[a,*], Jilin Huang[a], Mingwen Zhao[c], Jie Zhan[c], Chunhua Feng[a], Zhenghua Tang[a], Shaowei Chen[a,d], Hong Liu[b,c,**]

[a]*New Energy Research Institute, School of Environment and Energy, South China University of Technology, Guangzhou Higher Education Mega Center, Guangzhou, Guangdong 510006, China*
[b]*Beijing Institute of Nanoenergy and Nanosystems, Chinese Academy of Science, Beijing 100083, China*
[c]*State Key Laboratory of Crystal Materials, Center of Bio & Micro/Nano Functional Materials, Shandong University, 27 Shandanan Road, Jinan, Shandong 250100, China*
[d]*Department of Chemistry and Biochemistry, University of California, 1156 High Street, Santa Cruz, CA 95064, USA*

Received 22 March 2015; received in revised form 3 July 2015; accepted 10 July 2015
Available online 20 July 2015

KEYWORDS
Doped carbon;
Non-metal catalyst;
Biomass;
Electronic structure;
Hydrogen evolution reaction

Abstract
Development of non-metal catalysts for hydrogen evolution reaction (HER) with both excellent activity and robust stability has remained a key challenge in recent decades. Herein, sulfur and nitrogen self-doped carbon nanosheets are prepared as efficient non-metal catalysts for HER by thermal decomposition of peanut root nodules, an abundant biowaste. The obtained S and N-doped carbons exhibit a porous and multilayer structure with a specific surface area of 513.3 m^2/g and high electrochemical area of 27.4 mF/cm^2. Electrochemical measurements show apparent electrocatalytic activity for HER in 0.5 M H_2SO_4, with a small overpotential of only −0.027 V, a Tafel slope of 67.8 mV/dec and good catalytic stability. The density functional theory calculations confirmed that both S and N doping significantly change the electronic structure of carbon catalysts. However, after S-doping into carbon skeleton, the surrounding

*Corresponding author at: New Energy Research Institute, School of Environment and Energy, South China University of Technology, Guangzhou Higher Education Mega Center, Guangzhou, Guangdong 510006, China.
**Corresponding author at: Beijing Institute of Nanoenergy and Nanosystems, Chinese Academy of Science, Beijing 100083, China.
E-mail addresses: eszhouwj@scut.edu.cn (W. Zhou), hliu@binn.cas.cn (H. Liu).
[1]These authors contributed equally to the work.

http://dx.doi.org/10.1016/j.nanoen.2015.07.008

electric density of S atoms and C atoms increases, but after N-doping it only increases that of C atoms. The results presented herein may offer a novel and effective methodology for the design and engineering of efficacious and ecologically friendly catalysts for water splitting technology.

Introduction

Increasing global concerns over environmental issues and energy crisis have stimulated a great deal of interest in the development of novel technologies for clean and sustainable energy. Hydrogen has been widely considered as a promising fuel to address the environmental (pollution-free) and energy (high combustion value) concerns. Therefore, hydrogen evolution reaction (HER), the electrochemical reduction of water combined with wind and solar power, has attracted increasing attention recently [1–3]. In addition, highly active HER electrocatalysts as co-catalysts can observably enhance the efficiency of photocatalytic water splitting [4–8]. Pt-based electrocatalysts are known to effectively catalyze HER. However, the widespread application has been significantly hindered by the limited reserves and high costs [5,9]. Hence, development of sustainable HER catalysts that are composed of cost-effective and earth-abundant elements has been one of the main challenges in renewable energy research so far [10–12]. In fact, Mo-based sulfides, nitrides, carbides and selenides (e.g., MoS_2, Mo_2C, Ni–Mo–N and $MoSe_2$) [12–17], Co/Ni-based metal sulfides, selenides, phosphides (e.g., CoS_2, $CoSe_2$, CoP, and $Ni_{12}P_5$) [18–21] and other sulfides (TiS_2 and TaS_2) [22] have been prepared and examined as effective HER catalysts in a series of recent studies.

Currently, carbon coated metal nanoparticles (Co, Fe, Ni, Ag, etc.) [23–27] or carbon doped by all kinds of nonmetal elements (N, S, P, B, etc.) [28–31] represent one new class of effective HER catalysts. For instance, Zheng [32] observed unexpected HER activity with g-C_3N_4 loaded on N-doped graphene where the overpotential and Tafel slope were comparable to those of some of the well-developed metallic catalysts. In another study, Chen et al. [29] show that nitrogen and sulfur co-doped nanoporous graphene exhibited high catalytic activity in HER at low operating potentials, a performance comparable to that of MoS_2, arguably the best Pt-free HER catalyst. However, the synthetic process was rather expensive, complex, and tedious, involving the preparation of nanoporous Ni substrates and nanoporous graphene by CVD method. Despite these breakthroughs, the low cost and high-efficiency HER catalysts also need to be easily prepared on a large scale. In addition, a detailed understanding of the fundamental mechanism for doping carbon based HER catalysts has remained elusively thus far.

Herein, S and N doped carbon nanosheets are simply prepared on a large scale by thermal treatment of an abundant biomass, peanut root nodules, and examined their corresponding electrocatalytic activity for HER in acidic media. In the present study, by taking advantage of the rich sulfur and nitrogen contents in peanut root nodules, S and N self-doped porous carbons were produced by controlled pyrolysis at elevated temperatures, as manifested in various spectroscopic measurements. Electrochemical measurements showed that the resulting S and N doped porous carbon exhibited apparent HER activity with a low onset potential of only −0.027 V, a Tafel slope of 67.8 mV/dec and remarkable durability. Finally, DFT calculations confirmed that sulfur doping, rather than nitrogen doping, played a more important role in determining the HER activity.

Experimental section

Synthesis of porous carbons from peanut root nodules

Peanut root nodules were first washed with DI water for three times to remove impurities. 1 g of nodules and 3 g of $MgCl_2$ (as activating agent to increase the specific surface area of the obtained carbon [33,34]) were put into a ceramic boat, calcined at selected temperatures within the temperature range of 600–900 °C in an Ar atmosphere for 2 h, and cooled down to room temperature naturally. The black products were then washed with a 1 M HCl aqueous solution, which were denoted as RN-T with T being the calcination temperatures. Four samples were prepared, RN-600, RN-700, RN-800 and RN-900.

Synthesis of N-doped, N,S co-doped and S-doped carbons

Samples were prepared with different starting materials to study the effect of elementary composition on HER: (i) 1 g of sucrose, 0.05 g of dicyandiamide, (ii) 1 g of sucrose, 0.05 g of thiourea, and (iii) 1 g of sucrose, 0.05 g of sulfur powder, which were calcined at 800 °C for 2 h in an Ar atmosphere. 3 g of $MgCl_2$ was also used as activating agent in all calcination process. The resulting black products were washed with a 1 M HCl aqueous solution and the obtained porous carbon was donated as N-doped carbon (NC), N and S co-doped carbon (NSC) and S-doped carbon (SC), respectively.

Characterization

Field-emission scanning electron microscopic (FESEM, NOVA NanoSEM 430, FEI) measurements were used to characterize the morphologies of the obtained samples. Transmission electron microscopic (TEM) measurements were carried out with a JOEL JEM 2100F microscope. Powder X-ray diffraction (XRD) patterns of the samples were recorded on a Bruker D8 Advance powder X-ray diffractometer with Cu Kα (λ=0.15406 nm) radiation. X-ray photoelectron spectroscopic (XPS) measurements were performed using an ESCALAB 250. Raman spectra

were recorded on a RENISHAW inVia instrument with an Ar laser source of 488 nm in a macroscopic configuration. BET surface area was evaluated by using a Micromeritics ASAP 2010 instrument with nitrogen adsorption at 77 K and the Barrett–Joyner–Halenda (BJH) method.

Electrochemistry

Electrochemical measurements were performed with an electrochemical workstation (CHI 760C, CH Instruments Inc.) in a 0.5 M H_2SO_4 aqueous solution. A Hg/Hg_2Cl_2 electrode (saturated KCl) and a graphite rod were used as the reference and counter electrode, respectively. 4 mg of the catalyst powders was dispersed in 1 mL of 4:1 (v:v) water/ethanol mixed solvents along with 80 μL of a Nafion solution, and the mixture was sonicated for 30 min. Then, 5 μL of the above solution was dropcast onto the surface of a glassy carbon disk electrode at a catalyst loading of 0.285 mg/cm^2. The as-prepared catalyst film was dried at room temperature. Polarization curves were acquired by sweeping the potential between 0 and −0.8 V (vs. Hg/Hg_2Cl_2) at a potential sweep rate of 5 mV/s. The accelerated stability tests were performed in 0.5 M H_2SO_4 at room temperature by potential cycling between 0 and −0.6 V (vs. Hg/Hg_2Cl_2) at a sweep rate of 100 mV/s for a given number of cycles. Cyclic voltammetry (CV) can be used to probe the electrochemical double layer at nonfaradaic overpotentials as a means for estimating the effective electrode surface area. The potential range of 0.1 V with no redox peak was employed. The CV scan rates should be as large to minimize Faraday current, such as 40, 60, 80, 120, 160 and 200 mV/s. Current-time responses were monitored by chronoamperometric measurements for 12 h. Hydrogen production of S and N doped carbon

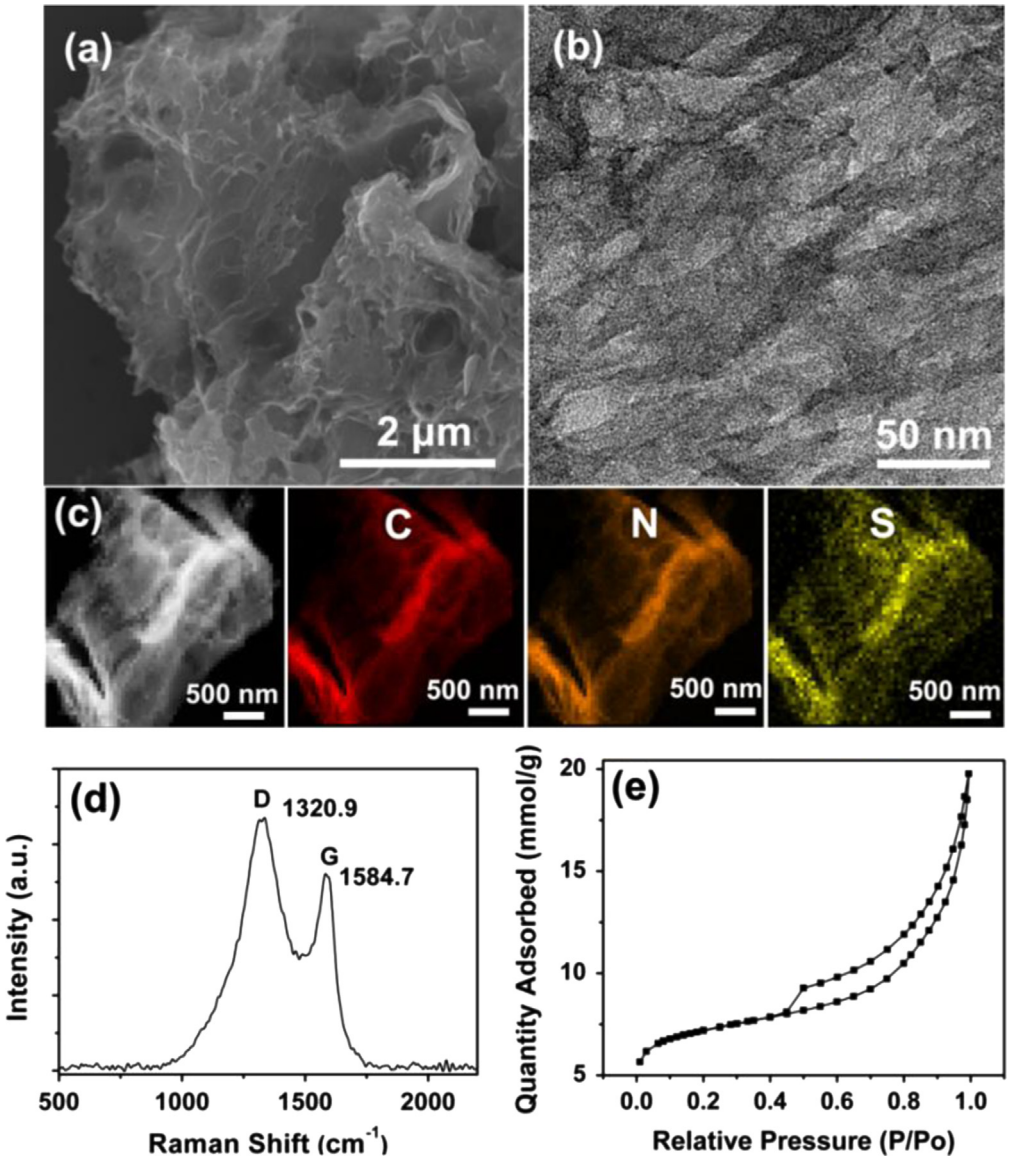

Figure 1 (a) SEM image, (b) TEM image, (c) EDS maps, (d) Raman spectrum and (e) nitrogen adsorption/desorption isotherm for RN-800.

nanosheets modified electrode was carried out at −0.33 V (vs. RHE) and the hydrogen gas production rate was quantified by gas chromatographic measurements (GC-2060F, LuNan Analytical Instruments, Ltd., China).

In all measurements, the Hg/Hg_2Cl_2 reference electrode (SCE) was calibrated with respect to a reversible hydrogen electrode (RHE). The calibration was performed in a high-purity H_2 (99.999%) saturated electrolyte with a Pt wires as the working electrode and counter electrode. Cyclic voltammograms (CVs) were collected at a scan rate of 1 mV/s, and the average of the two potentials at which the current crossed zero was taken as the thermodynamic potential for the hydrogen electrode reactions. In 0.5 M H_2SO_4, $E(RHE)=E(Hg/Hg_2Cl_2)+0.273$ V (Figure S1).

DFT calculations

All calculations were performed using the Vienna Ab-initio Simulation Package (VASP). The Perdew–Burke–Ernzerhof (PBE) functional for the exchange correlation term was used with the projector augmented wave method and a cutoff energy of 400 eV. To investigate the effect of nitrogen and sulfur doping, a carbon nanosheet doped with N or S atoms was used as the calculation model, respectively, and the density of states (DOS) was calculated. All structures were fully relaxed to the ground state.

Result and discussion

In this study, we developed a novel and simple approach to synthesize porous carbon nanosheets from peanut root nodules (Figure S2) by an effective thermal carbonization route. During carbonization at elevated temperatures under an Ar atmosphere, the carbon source formed a porous sheet structure (denoted as RN-T with T being the pyrolysis temperature), which was then subject to structural characterizations with a range of experimental techniques. Figure 1a and b depicts a representative SEM and TEM image of the sample prepared at 800 °C (RN-800), from which one can see that the sample exhibited a porous and multilayer structure with rather extensive stacking and folding. Mapping analysis based on energy-dispersive X-ray dispersive spectroscopy (EDS) (Figure 1c) confirmed that carbon nanosheets were formed and doped with both N and S elements. The graphitic characteristics of RN-800 were further confirmed by Raman measurements, where the D band at 1334.5 cm^{-1} and G band 1585.6 cm^{-1} can be clearly seen (Figure 1d). The former is assigned to the vibration of carbon atoms with dangling bonds in planar terminations of disordered graphite, and the latter to the E2g mode of 2D graphite [35,36]. The corresponding XRD patterns are shown in Figure S3, where the peak at $2\theta=26.5^{\circ}$ can be assigned as the diffraction of graphite (002) crystalline planes. No other crystalline impurities were detected. Nitrogen adsorption/desorption measurements showed a type IV isotherm with a

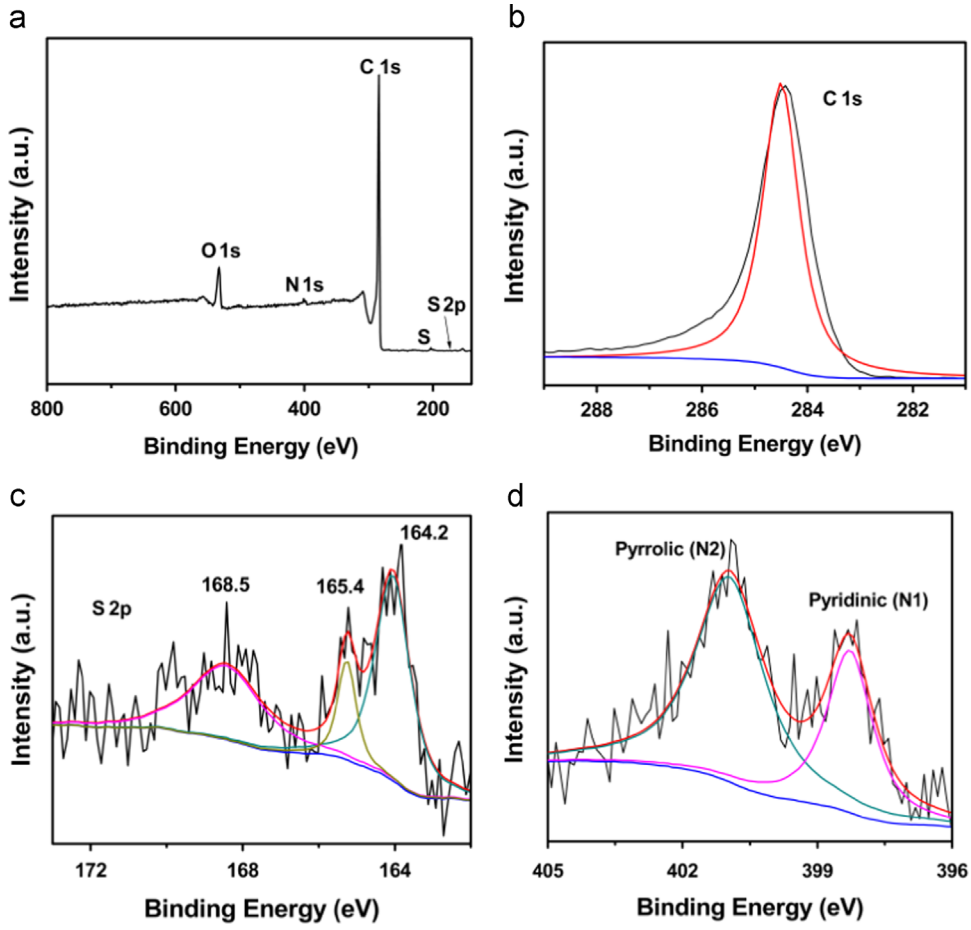

Figure 2 (a) XPS survey spectrum and high-resolution scans of (b) C1s, (c) S2p and (d) N electrons of RN-800.

clear H_2-type hysteresis loop in the relative pressure region of 0.4–1.0 P/P_0, from which a high specific surface area was estimated to be 513.3 m^2/g, indicating the formation of a mesoporous structure (Figure 1e).

XPS measurements were then carried out to analyze the surface chemistry of the obtained porous carbons. In the survey spectrum in Figure 2a, the elements of C, O, S, and N were detected in the RN-800 sample. High-resolution scan of carbon shows a major peak at 284.5 eV that is characteristic of C1s (Figure 2b). Deconvolution of the high-resolution scan of the S2p electrons yielded three peaks at the binding energies of 164.2 eV, 165.4 eV and 168.5 eV (Figure 2c). The first two signified the incorporation of sulfur into the graphitic matrix forming C–S bonds whereas the last one might be assigned to oxidized sulfur species of C-SO_x-C (x=2 or 3) groups [37]. Additionally, the N1s spectrum (Figure 2d) can be deconvoluted into two peaks centered at 398.3 and 401.1 eV, which are consistent with pyridinic (N1) and pyrrolic (N2) nitrogens, respectively. This indicates that nitrogen was also doped into the carbon molecular skeleton. Furthermore, based on the integrated peak areas of the S2p and N1s peaks, the atomic contents of S and N in RN-800 were estimated to be 0.27 and 2.02 at%, respectively.

The electrocatalytic activities for HER were then examined by electrochemical measurements in 0.5 M H_2SO_4. From Figure 3a, one can see that with a glassy carbon electrode modified with a calculated amount of RN-800, apparent non-zero cathodic currents started to emerge when the electrode potential was more negative than −0.027 V (vs. RHE), which is only somewhat more negative than that (−0.004 V) of commercial 20 wt% Pt/C catalysts at the same catalyst loading. In addition, to reach a current density of 10 mA/cm^2, an overpotential of −116 mV was required with RN-800, as compared to −0.031 V for Pt/C. In addition, the linear portions of the polarization curves were fitted to the Tafel equation ($\eta = b \log j + a$, where j is the current density and b is the Tafel slope), yielding Tafel slopes of 67.8 mV/dec for RN-800 and 31.6 mV/dec for 20 wt% Pt/C (Figure 3b). Note that a lower Tafel slope suggests a more drastic increase of HER currents with increasing electrode potential and hence a better HER performance. For hydrogen evolution in acid on catalyst surfaces, the mechanism typically involves three major reactions [38,39]

$$H_3O^+ + e \leftrightarrow H^* + H_2O \text{ (Volmer reaction, } b=120 \text{ mV/dec)} \quad (1)$$

$$2H^* \leftrightarrow H_2^* \text{(Tafel reaction, } b=30 \text{ mV/dec)} \quad (2)$$

$$H_3O^+ + e + H^* \leftrightarrow H_2^* + H_2O \text{ (Heyrovsky reaction, } b=40 \text{ mV/dec)} \quad (3)$$

where H* and H_2* represent a hydrogen atom and molecule adsorbed on to a surface atom, respectively. Thus, one can see that whereas the HER performance was primarily limited by the Tafel reaction at Pt/C (Eq. (2)), the rate-determining step at RN-800 most probably involved both electroreduction of protons into H* (Eq. (1)) and the subsequent formation of H_2* (Eq. (2)).

It should be noted that such an HER performance of RN-800 (onset potential −0.027 V, 59.4 mA/cm^2 at −0.2 V vs. RHE, b=67.8 mV/dec) is actually markedly better than or comparable to those of leading Mo-based HER catalysts (Table S1), such as MoS_2/reduced graphene (−0.10 V, 48 mA/cm^2 at −0.2 V vs. RHE, 41 mV/dec) [11], $NiMoN_x$/C nanosheets (−0.078 V, 13 mA/cm^2 at −0.2 V vs. RHE, 35.9 mV/dec) [12], defect-rich MoS_2 nanosheets (−0.12 V, 4 mA/cm^2 at −0.2 V vs. RHE, 50 mV/dec) [10], WS_2 nanosheets (−0.080 V, 5.5 mA/cm^2 at −0.2 V vs. RHE, 60 mV/dec) [3], carbon-based HER catalysts, such as cobalt-embedded nitrogen-rich carbon nanotubes (−0.05 V, 6 mA/cm^2 at −0.2 V vs. RHE, 80 mV/dec) [23], g-C_3N_4 nanoribbon-graphene (−0.08 V, 10 mA/cm^2 at −0.2 V vs. RHE, 54 mV/dec) [30], C_3N_4@N-doped graphene (−0.12 V, 10 mA/cm^2 at −0.24 V vs. RHE, 51.5 mV/dec) [32], and N and S co-doped nanoporous graphene (−0.14 V, 10 mA/cm^2 at −0.39 V vs. RHE, 80.5 mV/dec) [29]. This suggests that the porous carbons derived from controlled pyrolysis of peanut root nodules might indeed serve as effective HER catalysts.

Electrochemical impedance spectroscopy (EIS) measurements were then carried out to further probe the electron-transfer kinetics involved. Figure 3c depicts the Nyquist plots of the RN-800 modified electrode at various overpotentials, where one can see that the diameter of the semicircles, i.e., the charge-transfer resistance (Rct), diminished markedly with increasing overpotential. More detailed analyses were carried out by fitting the impedance data to an equivalent circuit depicted in the inset to Figure 3c, where Rs represents uncompensated solution resistance, Rct is the charge-transfer resistance and CPE is the constant-phase element. Indeed, Rct decreased significantly with increasing overpotentials, from 402.6 Ω at −100 mV to 72.4 Ω at −150 mV. Note that these values are drastically lower than those of other HER catalysts at similar overpotentails, such as MoS_2 on mesoporous graphene (1810 Ω at −90 mV) [40], and WS_2 nanoribbons (38 Ω at −250 mV) [41].

Typically, the current density is expected to be proportional to catalytically active surface area. Another alternative approach to estimate the effective surface area is to measure the capacitance of the double layer at the solid−liquid interface with cyclic voltammetry, which were shown in Figure 3d and e. The high electrochemical area of RN-800 modified electrode is 27.4 mF/cm^2, which is mainly due to the high specific surface area of porous carbon nanosheets. It is worth noting that a rectangular shape in all CV curves was maintained when the scan rate increased from 40 mV/s to 200 mV/s, suggesting facile ion transport and good ionic conductivity, which agrees with the electrochemical impedance results (Figure 3c).

In addition to excellent catalytic activity, the RN-800 modified electrode also exhibited extraordinary stability in HER. Figure 3f shows that even after 1000 continuous potential cycles, the j-V curve of the RN-800 electrode remained almost unchanged, suggesting long-term viability under operating conditions. To further investigate the stability of RN-800 in HER, the current-time plots at the applied potential of −0.25 V (vs. RHE) was depicted in the inset to Figure 3f. One can see that the current remain almost invariable over 12 h of continuous operation. The generated gas was collected and confirmed to be hydrogen by gas chromatography, and the hydrogen produced amounts were shown in Figure S4. Linear regressions of the experimental data yield the corresponding hydrogen production rate is ~438 mmol g^{-1} h^{-1}, which is similar with or better than that of the reported results, such as three-dimensional

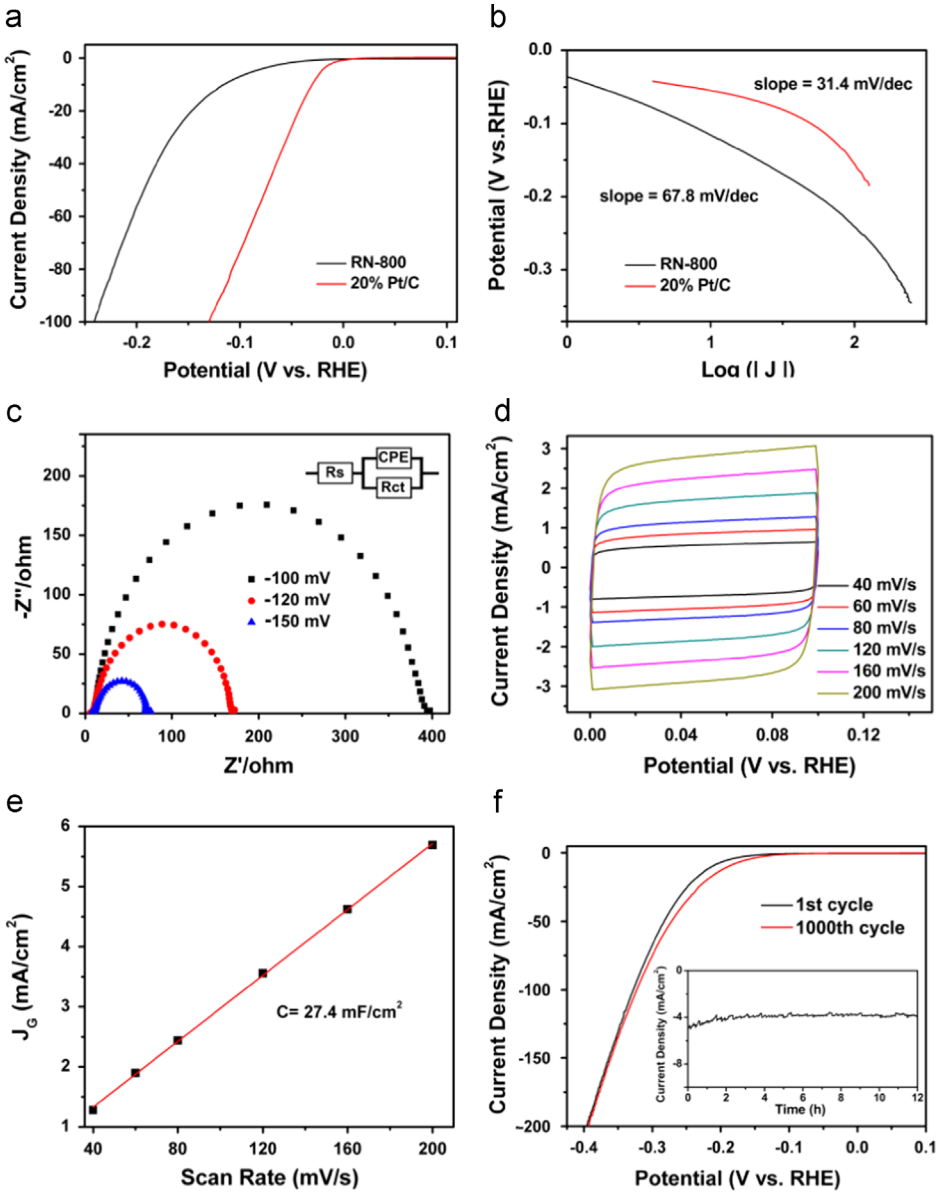

Figure 3 (a) Polarization curves for HER in 0.5 M H_2SO_4 at a glassy carbon electrode modified with RN-800 or 20 wt% Pt/C. Potential sweep rate 5 mV/s. (b) Corresponding Tafel plots derived from (a). (c) Nyquist plots and the equivalent circuit of the RN-800 modified electrode at various HER overpotentials in 0.5 M H_2SO_4. (d) Cyclic voltammograms (CV) taken in a potential window without faradaic processes and (e) the capacitive currents at 0.05 V vs. RHE as a function of scan rate for RN-800 electrodes. (f) HER polarization curves for RN-800 before and after 1000 cycles of potential sweeps. Inset shows the current-time plot at the applied potential of −0.25 V (vs. RHE).

MoS_2/graphene frameworks (358.2 mmol g^{-1} h^{-1} at −0.236 V vs. RHE), porous metallic MoO_2-supported MoS_2 nanosheets (120 mmol g^{-1} h^{-1} at −0.23 V vs. RHE) and MoS_x grown on graphene-protected 3D Ni foams (13.47 mmol g^{-1} cm^{-2} h^{-1} at −0.2 V vs. RHE) [42].

The effects of carbonization temperature on the morphologies and structure of RN were also examined. SEM studies (Figure 4a-c) showed similar sheet-like morphologies of the RN samples prepared at different annealing temperatures (600 °C, 700 °C, 800 °C, and 900 °C). Raman measurements (Figure 4d) suggested increasing regularity of the porous carbons with the calcination temperature increased from 600 °C to 900 °C, as manifested with a monotonic decrease of the I_D/I_G ratio. More significantly, XPS measurements (Figure S5) indicated that the bonding configurations of S dopants in carbon catalysts were different. The RN samples obtained at low temperature (600 °C), the sulfone groups were the major oxidized sulfur moieties, which induced the lower HER activity (Figure 4f). Overall it can be seen that the concentrations of oxidized sulfur moieties decreased and the C–S bonds increased with increasing pyrolysis temperature from 600 °C to 800 °C. The corresponding HER catalytic activities increased, as seen from the gradual decrease in the overpotentials from

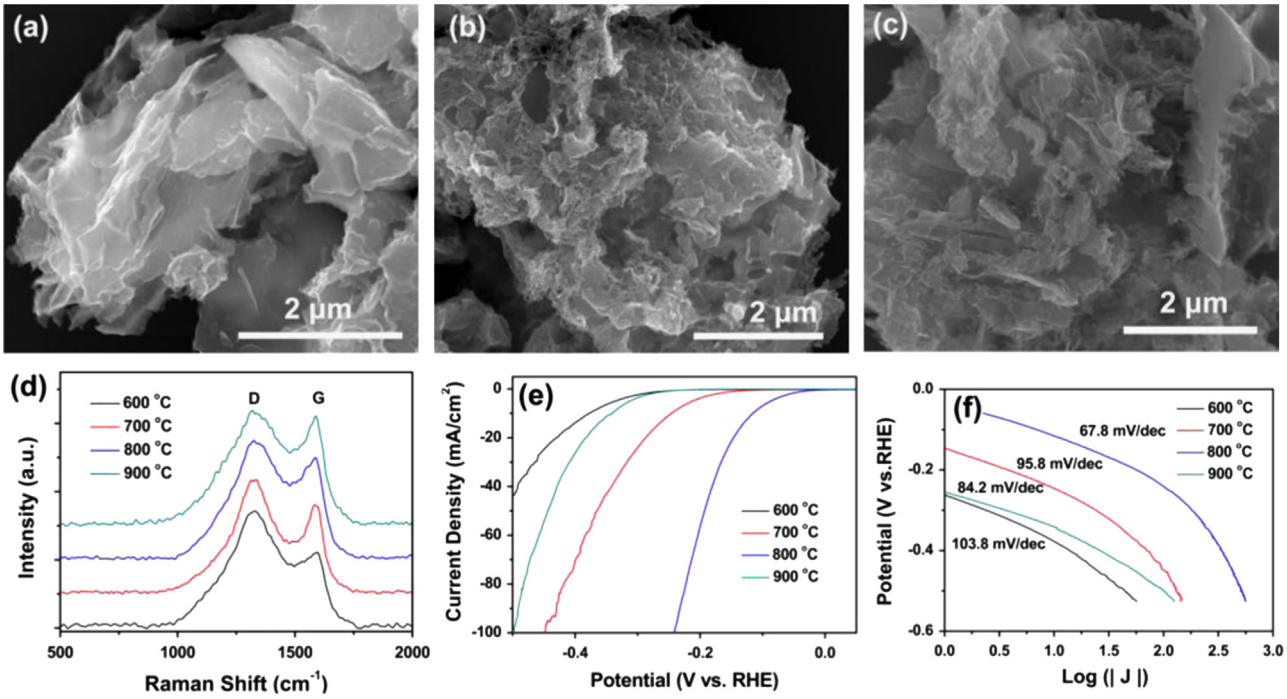

Figure 4 The SEM images of RN obtained at different temperatures. (a) 600 °C, (b) 700 °C, and (c) 900 °C, (d) Raman result, (e) polarization curves and (f) corresponding Tafel plots derived from (e) of RN obtained at different temperatures.

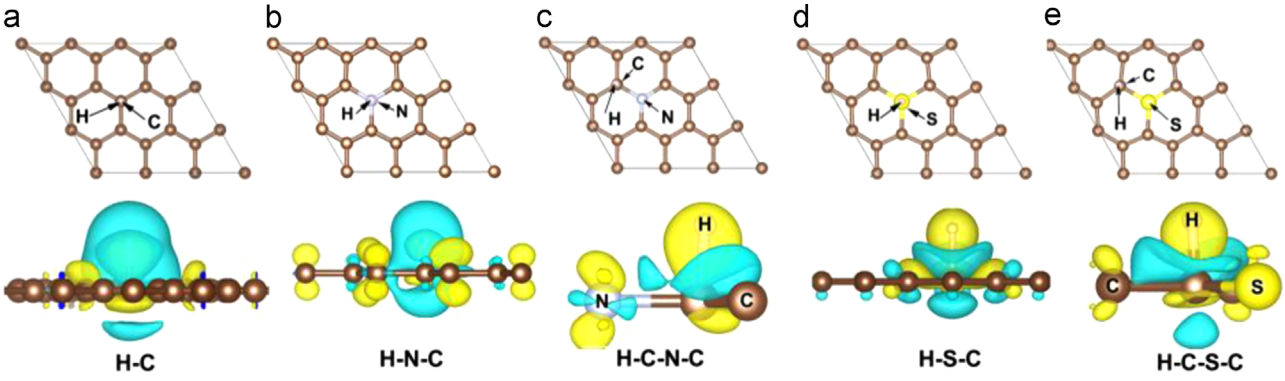

Figure 5 Structural models and charge density of H adsorbed on the surface of graphene, N-doped graphene and S-doped graphene. (a) H atom was combined on the C atom; H atom was combined on the N (b) or S (d) dopant atom; H atom was combined on the C atom around N (c) or S (e) dopant atom. The blue and yellow symbols denote decreased and increased charge density, respectively.

−0.271 V to −0.027 V (Figure 4e). The catalytic activity of the materials with low S doping obtained at 900 °C decrease, with overpotential of about −0.253 V, due to the decomposition at high temperature. The linear portions of Tafel plots were fitted to the Tafel equation, yielding Tafel slopes of 103.8 mV/dec, 95.8 mV/dec, 67.8 mV/dec and 84.2 mV/dec for RN-600 °C, RN-700 °C, RN-800 °C, and RN-900 °C, respectively (Figure 4f). The results confirm that the C–S bonds in doped carbon play an important role in enhancing the HER activity.

The effect of S and N doping into carbon on HER was confirmed by density functional theory (DFT) calculations (Figure 5). The calculation was focused on hydrogen atom binding energy on catalyst, an important intermediate state in HER (Eqs. (1)-(3)) [11,38,39]. The structural models of H adsorbed on the different binding sites on pristine graphene, S-doped graphene, and N-doped graphene were constructed. For N-doped graphene, the charge density of the N–H bond diminished because of spilling of electrons to the nearby carbon atoms (Figure 5b) and the charge density increases only on C atoms neighboring N doping atoms (Figure 5c). By comparison, for S doped graphene, it can be seen from Figure 5d and e that electrons were transferred from S-doped graphene to H, which increased the charge density of the S—H bond. This suggests that the stabilization of the H* species in HER may originate from the enhanced charge

density of S-doped carbon atoms, where S atoms are inherently advantageous in interacting with H^+ than carbon atoms due to the lone-pair electrons. It is worth noting whether H absorbed onto C or S, the charge density was increased and enhanced hydrogen atom binding energy on catalyst. In summary, DFT calculations strongly suggest that S-doping into the carbon matrix led to enhanced adsorption of H on S doping atoms and the neighboring C atoms, whether H was absorbed on S or C in the C–S bonds. The DFT calculations implied that the S doping into carbon based catalysts could be more efficiently to enhance the HER activity than that of N doping.

In order to demonstrate the calculation model, the additional experiments were also conducted to obtain some insights into the origin of the superior catalytic activity as well as their elementary composition-catalytic activity relationships. In our experiment, the sucrose ($C_{12}H_{22}O_{11}$, only composed of C, H and O) as carbon source was used to synthesize N-doped carbon (NC) by adding dicyandiamide, N and S co-doped carbon (NSC) by adding thiourea and S-doped carbon (SC) by adding sulfur powder. The similar carbon nanosheets are shown in SEM images (Figure S6). The electrocatalytic activities of the different materials toward HER clearly indicate that the catalytic activities increase in the order of NC (onset potential of −0.241 V, vs. RHE), NSC (−0.135 V), and SC (−0.041 V), as shown in Figure S7a. The corresponding Tafel plots are shown in Figure S7b, which are 122 mV/dec for NC, 84 mV/dec for NSC and 54.7 mV/dec for SC, which further illustrate that the S doping play a pivotal role in enhancing the HER activity of carbon.

Conclusion

n this study, an earth-abundant biowaste, peanut root nodules was used to prepare effective non-metal HER electrocatalysts by controlled pyrolysis at elevated temperatures. With the rich sulfur and nitrogen contents in the root nodules, both S and N were doped into the molecular skeletons of the resulting porous carbons. TEM and SEM measurements exhibited a porous and multilayer structure with a specific surface area up to 513.3 m^2/g. Electrochemical measurements showed that the sample prepared at 800 °C displayed the best HER activity among the series, with a small onset potential of only −0.027 V (vs. RHE), a Tafel slope of 67.8 mV/dec, a large catalytic current density of 59.4 mA/cm^2 at −0.2 V, and prominent electrochemical durability. Such a performance, while somewhat subpar as compared to that of commercial Pt/C, was markedly better than those of leading Mo-based HER catalysts. DFT calculations confirmed that S doping led to marked changes of the electronic energy structures and enhanced adsorption of H atoms on the catalysts, which more efficiently to enhance the HER activity than that of N doping. The results presented herein may offer a novel and effective methodology for the preparation of non-metal HER catalysts based on abundant biowastes on a large scale.

Acknowledgments

This work was supported by the National Recruitment Program of Global Experts, the Ph.D. Start-up Funds of the Natural Science Foundation of Guangdong Province (S2013040016465), Project of Public Interest Research and Capacity Building of Guangdong Province (2014A010106005) and Zhujiang New Stars of Science & Technology (2014J2200061). J. Z. thanks the NSFC for financial support (grant No. 51372138). The authors would also like to thank the National Super Computing Centre in Jinan for assistance in theoretical calculations.

Appendix A. Supporting information

Supplementary data associated with this article can be found in the online version at http://dx.doi.org/10.1016/j.nanoen.2015.07.008.

References

[1] R. Subbaraman, D. Tripkovic, D. Strmcnik, K.-C. Chang, M. Uchimura, A.P. Paulikas, V. Stamenkovic, N.M. Markovic, Science 334 (2011) 1256–1260.
[2] W. Zhou, X.-J. Wu, X. Cao, X. Huang, C. Tan, J. Tian, H. Liu, J. Wang, H. Zhang, Energy Environ. Sci. 6 (2013) 2921–2924.
[3] D. Voiry, H. Yamaguchi, J. Li, R. Silva, D.C. Alves, T. Fujita, M. Chen, T. Asefa, V.B. Shenoy, G. Eda, M. Chhowalla, Nat. Mater. 12 (2013) 850–855.
[4] X. Zong, H. Yan, G. Wu, G. Ma, F. Wen, L. Wang, C. Li, J. Am. Chem. Soc. 130 (2008) 7176–7177.
[5] Q. Xiang, J. Yu, M. Jaroniec, J. Am. Chem. Soc. 134 (2012) 6575–6578.
[6] W. Zhou, Z. Yin, Y. Du, X. Huang, Z. Zeng, Z. Fan, H. Liu, J. Wang, H. Zhang, Small 9 (2013) 140–147.
[7] K. Chang, Z. Mei, T. Wang, Q. Kang, S. Ouyang, J. Ye, ACS Nano 8 (2014) 7078–7087.
[8] J. Chen, X.-J. Wu, L. Yin, B. Li, X. Hong, Z. Fan, B. Chen, C. Xue, H. Zhang, Angew. Chem. Int. Ed. 54 (2015) 1210–1214.
[9] I.E.L. Stephens, I. Chorkendorff, Angew. Chem. Int. Ed. 50 (2011) 1476–1477.
[10] J. Xie, H. Zhang, S. Li, R. Wang, X. Sun, M. Zhou, J. Zhou, X.W. Lou, Y. Xie, Adv. Mater. 25 (2013) 5807–5813.
[11] Y. Li, H. Wang, L. Xie, Y. Liang, G. Hong, H. Dai, J. Am. Chem. Soc. 133 (2011) 7296–7299.
[12] W.F. Chen, K. Sasaki, C. Ma, A.I. Frenkel, N. Marinkovic, J.T. Muckerman, Y. Zhu, R.R. Adzic, Angew. Chem. Int. Ed. 51 (2012) 6131–6135.
[13] C.-B. Ma, X. Qi, B. Chen, S. Bao, Z. Yin, X.-J. Wu, Z. Luo, J. Wei, H.-L. Zhang, H. Zhang, Nanoscale 6 (2014) 5624–5629.
[14] X. Huang, Z. Zeng, S. Bao, M. Wang, X. Qi, Z. Fan, H. Zhang, Nat. Commun. 4 (2013) 1444.
[15] W. Zhou, K. Zhou, D. Hou, X. Liu, G. Li, Y. Sang, H. Liu, L. Li, S. Chen, ACS Appl. Mater. Interfaces 6 (2014) 21534–21540.
[16] H. Vrubel, X. Hu, Angew. Chem. Int. Ed. 124 (2012) 12875–12878.
[17] C. Xu, S. Peng, C. Tan, H. Ang, H. Tan, H. Zhang, Q. Yan, J. Mater. Chem. A 2 (2014) 5597–5601.
[18] Z. Huang, Z. Chen, Z. Chen, C. Lv, H. Meng, C. Zhang, ACS Nano 8 (2014) 8121–8129.
[19] E.J. Popczun, C.G. Read, C.W. Roske, N.S. Lewis, R.E. Schaak, Angew. Chem. Int. Ed. 53 (2014) 5427–5430.
[20] E.J. Popczun, J.R. McKone, C.G. Read, A.J. Biacchi, A.M. Wiltrout, N.S. Lewis, R.E. Schaak, J. Am. Chem. Soc. 135 (2013) 9267–9270.
[21] D. Kong, H. Wang, Z. Lu, Y. Cui, J. Am. Chem. Soc. 136 (2014) 4897–4900.

[22] Z. Zeng, C. Tan, X. Huang, S. Bao, H. Zhang, Energy Environ. Sci. 7 (2014) 797–803.
[23] X. Zou, X. Huang, A. Goswami, R. Silva, B.R. Sathe, E. Mikmeková, T. Asefa, Angew. Chem. Int. Ed. 126 (2014) 4461–4465.
[24] J. Deng, P. Ren, D. Deng, X. Bao, Angew. Chem. Int. Ed. 54 (2015) 2100–2104.
[25] Y. Hou, Z. Wen, S. Cui, S. Ci, S. Mao, J. Chen, Adv. Funct. Mater. 25 (2015) 872–882.
[26] W. Zhou, J. Zhou, Y. Zhou, J. Lu, K. Zhou, L. Yang, Z. Tang, L. Li, S. Chen, Chem. Mater. 27 (2015) 2026–2032.
[27] W. Zhou, Y. Zhou, L. Yang, J. Huang, Y. Ke, K. Zhou, L. Li, S. Chen, J. Mater. Chem. A 3 (2015) 1915–1919.
[28] M. Shalom, S. Gimenez, F. Schipper, I. Herraiz-Cardona, J. Bisquert, M. Antonietti, Angew. Chem. Int. Ed. 126 (2014) 3728–3732.
[29] Y. Ito, W. Cong, T. Fujita, Z. Tang, M. Chen, Angew. Chem. Int. Ed. 54 (2015) 2131–2136.
[30] X. Huang, Y. Zhao, Z. Ao, G. Wang, Sci. Rep. 4 (2014) 7557.
[31] Y. Zheng, Y. Jiao, L.H. Li, T. Xing, Y. Chen, M. Jaroniec, S.Z. Qiao, ACS Nano 8 (2014) 5290–5296.
[32] Y. Zheng, Y. Jiao, Y. Zhu, L.H. Li, Y. Han, Y. Chen, A. Du, M. Jaroniec, S.Z. Qiao, Nat. Commun. 5 (2014) 3783.
[33] F. Cesano, M.M. Rahman, S. Bertarione, J.G. Vitillo, D. Scarano, A. Zecchina, Carbon 50 (2012) 2047–2051.
[34] L. Sun, C. Tian, M. Li, X. Meng, L. Wang, R. Wang, J. Yin, H. Fu, J. Mater. Chem. A 1 (2013) 6462–6470.
[35] A.C. Ferrari, D.M. Basko, Nat. Nanotechnol. 8 (2013) 235–246.
[36] M.S. Dresselhaus, M. Terrones, Proc. IEEE 101 (2013) 1522–1535.
[37] Y.X. Huang, S.L. Candelaria, Y.W. Li, Z.M. Li, J.J. Tian, L. L. Zhang, G.Z. Cao, J. Power Sources 252 (2014) 90–97.
[38] W. Zhou, D. Hou, Y. Sang, S. Yao, J. Zhou, G. Li, L. Li, H. Liu, S. Chen, J. Mater. Chem. A 2 (2014) 11358–11364.
[39] J.G.N. Thomas, Trans. Faraday Soc. 57 (1961) 1603–1611.
[40] L. Liao, J. Zhu, X. Bian, L. Zhu, M.D. Scanlon, H.H. Girault, B. Liu, Adv. Funct. Mater. 23 (2013) 5326–5333.
[41] M.A. Lukowski, A.S. Daniel, C.R. English, F. Meng, A. Forticaux, R.J. Hamers, S. Jin, Energy Environ. Sci. 7 (2014) 2608–2613.
[42] Y.-H. Chang, C.-T. Lin, T.-Y. Chen, C.-L. Hsu, Y.-H. Lee, W. Zhang, K.-H. Wei, L.-J. Li, Adv. Mater. 25 (2013) 756–760.

Yucheng Zhou has been studying in college of Environment and Energy, South China University of Technology, since 2012. He will obtain a bachelor degree in 2016. He has been doing experiments with Dr. Weijia Zhou in New Energy Research Institute. His research interest is electro-catalytic water splitting and oxygen reduction.

Yanhua Leng obtained his B.Sc. degree from Shandong University in 2012. Currently, he is pursuing his M.Sc. degree under the supervision of Prof. Hong Liu in State Key Laboratory of Crystal Materials, Shandong University, China. His research is mainly focused on the first-principle calculation and crystal growth simulation.

Dr. Weijia Zhou completed his Ph.D. with Prof. Hong Liu and Prof. Jiyang Wang at Shandong University in 2012. He was doing research in Prof. Hua Zhang's group at Nanyang Technological University in 2011. Now, he is working in New Energy Research Institute, School of Environment and Energy, South China University of Technology, China. His research interests are related to the design and synthesis of low dimensional nanomaterials for new energy conversion and storage, including photo and electro-catalytic water splitting, supercapacitor and oxygen reduction reaction.

Jilin Huang has been studying in School of Environment and Energy, South China University of Technology, since 2012. And he will obtain a B.Sc. degree in 2016. Now, he is doing experiments in New Energy Research Institute with Dr. Weijia Zhou. His research interest is electro-catalytic water splitting.

Dr. Mingwen Zhao received his Ph.D. in 2001 at Shandong University. He is currently a professor of School of Physics at Shandong University. He has published more than 200 peer reviewed papers, such as Phys. Rev. Lett, Adv. Mater., Nano Letters, etc. He was also awarded by the State Ministry of Education of China for the outstanding research. His research interests are focused on the theoretical design of electronic structures of nanomaterials from first-principles which are closely related to applications in spintronics devices and energy generation.

Dr. Jie Zhan obtained his Ph.D. at Shandong University. He is associate professor in State Key Laboratory of Crystal Materials, Shandong University. His current research interests include synthesis and microstructure characterization of functional micro/nano crystals materials.

Dr. Chunhua Feng graduated with a Ph.D. degree in Chemical Engineering from Hong Kong University of Science and Technology in 2007. Dr. Feng is now a professor at School of Environment and Engineering, South China University of Technology (SCUT), China. He is serving as an associate director for Center of Environment Science, SCUT. He was elected in Program for New Century excellent talents in University, Ministry of Education, China (2012). His research interests lie in (1) energy/resource recovery from wastes; and (2) development of bioelectrochemical technology for wastewater treatment.

Dr. Zhenghua Tang obtained his B. S. degree at College of Chemistry and Chemical Engineering, Lanzhou University, Lanzhou, China in 2005. He attended graduate school there from 2005 to 2007. In August 2007, he moved to US and completed his Ph.D. study in Department of Chemistry, Georgia State University. After he received his Ph.D. degree, he did his postdoctoral training at Department of Chemistry, University of Miami from 2012 to 2014. He started his current position as associate professor at South China University of Technology since August, 2014. His research focuses on metal nanoclusters, nanocatalyst, electrochemistry, and peptide based bio-inspired nanomaterials.

Dr. Shaowei Chen obtained a B.Sc. degree from the University of Science and Technology of China, and then went to Cornell University receiving his M.Sc. and Ph.D. degrees in 1993 and 1996. Following a postdoctoral appointment in the University of North Carolina at Chapel Hill, he started his independent career in Southern Illinois University in 1998. In 2004, he moved to the University of California at Santa Cruz and is currently a Professor of Chemistry. He is also an adjunct professor at South China University of Technology. His research interest is primarily in the electron transfer chemistry of nanoparticle materials.

Dr. Hong Liu is professor in State Key Laboratory of Crystal Materials, Shandong University, and adjunct professor in Beijing Institute of Nanoenergy and Nanosystem, CAS. He has published over 250 peer reviewed paper, such as, Adv. Mater., J. Am. Chem. Soc., Nano Letters, etc., and published more than 25 patents. He was awarded as Distinguished Young Scholar by NNSF and Professor of Hundred Talents Program of CAS. His current research is focused mainly on nonlinear crystal growth, chemical processing of nanomaterials for energy related applications including photocatalysis, tissue engineering, especially the interaction between stem cell and nanostructure of biomaterials.